The CCL7-CCL2-CCR2 Axis Regulates Age-Related Alterations in ADSCs

Keya Li
Peking Union Medical College Comparative Medicine Center: Chinese Academy of Medical Sciences Institute of Laboratory Animal Sciences https://orcid.org/0000-0002-9248-8319

Guiying Shi
Peking Union Medical College Comparative Medicine Center: Chinese Academy of Medical Sciences Institute of Laboratory Animal Sciences

Xuepei Lei
Peking Union Medical College Comparative Medicine Center: Chinese Academy of Medical Sciences Institute of Laboratory Animal Sciences

Yiying Huang
Peking Union Medical College Comparative Medicine Center: Chinese Academy of Medical Sciences Institute of Laboratory Animal Sciences

Xinyue Li
Peking Union Medical College Comparative Medicine Center: Chinese Academy of Medical Sciences Institute of Laboratory Animal Sciences

Lin Bai (bailin49@163.com)
Peking Union Medical College Comparative Medicine Center: Chinese Academy of Medical Sciences Institute of Laboratory Animal Sciences https://orcid.org/0000-0002-0646-0812

Chuan Qin
Peking Union Medical College Comparative Medicine Center: Chinese Academy of Medical Sciences Institute of Laboratory Animal Sciences

---

Research

Keywords: ADSCs, Autologous stem cell transplantation, Aging, Chemokine, Cell cycle, Cell culture

Posted Date: April 6th, 2021

DOI: https://doi.org/10.21203/rs.3.rs-390571/v1

Abstract

Background and Objectives

Adipose-tissue derived stem cells (ADSCs) autologous transplantation have been a promising strategy for aging-related disorder. But the relationship between ADSCs senescence and organismal aging were still no consistent conclusions. Toward this end, we analyzed the senescence properties of ADSCs from different age donors to furthermore understand the differences of cells between young and senile donors and verify the influence of organismal aging on the proliferation and function of ADSCs in vitro, providing the theoretical basis for the clinical application of autologous ADSCs transplantation.

Methods and Results

We detected the characteristics, function, gene expression, apoptosis, cell cycle, SA-β-gal staining, and transcription features of ADSCs from 1-month mice and 20-month mice. ADSCs from old donors had some senescence-associated changes with less ability to proliferation than ADSCs from 1-month mice. Differentiation ability, cell surface markers, and SA-β-Gal staining did not differ across donor age, while cells exhibit a more remarkable age-related changes through continuous passages. According to the results of transcriptome analysis, the CCL7-CCL2-CCR2 axis and Hippo signaling pathway would be considered as its possible mechanisms.

Conclusions

Our study reveals that ADSCs from old donors have some age-related alterations. The CCL7-CCL2-CCR2 which lies behind this change would be a potential target for gene therapy to reduce harmful effects of ADSCs from old donors. To make autologous transplantation work better, we would recommend that ADSCs should be cryopreserved in youth with minimum number of passages.

Background

Aging is a multi-factorial phenomenon and extremely complex process that affects biological functions of organism, generally culminating in disease and death due to the accumulated actions of different types of stresses[1,2]. Age-associated pathologies, including neurodegenerative diseases, cardiovascular disorders, and certain metabolic diseases are common diseases associated with the aging process that can severely affect patients' daily life and represent a major economic challenge for families and society[3]. With the growing aging population, the issues of cognitive and behavioral dysfunction are becoming more of a concern[4].

Autologous stem cell transplantation is of particular effective method and has been a standard first-line therapy used in plasma cell dyscrasia, Parkinson's disease, amyotrophic lateral sclerosis(ALS) patients[5–8], which could eliminate the post-engrafting immunological rejection. With less ethical concerns when

used, adult stem cells are the main source of autologous transplantation that maintain the tissue homeostasis throughout whole life[9].

Zuk first isolated and identified adipose-tissue derived stem cells (ADSCs) from adipose tissue[10,11], and since then, research on ADSCs has rapidly advanced. ADSCs are advantageous for therapeutic use not only because of their plasticity but also because a sufficient number of ADSCs can be easily collected by minimally invasive surgical techniques[12,13]. ADSCs have enormous potential in vitro amplification, and differentiative capacity into several specific cells like neuronal cells, muscle epithelial cells, cardiac myocytes, osteoblasts, chondrocytes[14–20]. ADSCs present cell surface markers including CD10, CD13, CD29, CD44, CD71, CD73, CD90, CD105, CD166, CD271, while lack of CD14, CD34, CD45, CD11b[21,22]. ADSCs have immunomodulatory effect, secreting a variety of cytokines and have abilities of anti-apoptosis, anti-oxidation, anti-inflammatory[23,24].

As a promising source of autologous cell therapy for neurodegenerative diseases with the lower immunogenicity, it is unknown whether ADSCs from aging donors have the same therapeutic effect as the youngers. Also, the relationship between ADSCs and senescence in the existing literatures were still no consistent conclusions. Schultz argued that the number of cells and their capabilities decrease over time when organism senescence occurred, while stem cells pools maintain good stem cell characteristics with number of stem cells gradually deplete[25]. Schipper believed that the production, proliferation rate and pluripotency of adipose-derived stem cells in the young were superior to those of the elderly[26]. Alt confirmed that the expression of senescence genes of adipose-derived stem cells increased with age, while the miRNA which is related to the cell cycle regulating, apoptosis and the ability of maintenance homeostasis decreased[27]. Shi[28] and Zhu[29] show that age does not affect the ability of ADSCs in proliferate and differentiation. Aust[30] confirmed that the senescence of ADSCs is unrelated to age. And Mojallal[31] proved that the yield and proliferative capacity of adipose-derived stem cells were unrelated to age.

To further examine the correlation of organism aging and cell senescence, we isolated ADSCs from 1-month mice and 20-month mice to analyze the characteristics of ADSCs with age. The morphology, ultrastructure, proliferation, differentiation, function of secreting cytokines, surface markers, apoptosis, cell cycle, senescence-associated β-galactosidase (SA-β-gal) staining, and gene expression of ADSCs in these two age groups were detected. To gain a better understanding of its underlying mechanism, we investigated the two groups of ADSCs from mice (mADSCs) through the transcriptome sequencing (RNA-seq).

Methods

Mice

We purchased 1-month-age SPF-grade C57BL/6 mice from Beijing HFK Bio-Technology Co.,Ltd. The 20-month-age mice were from the experimental animal workshop. All animal experiments were conducted in accordance with accepted standards of animal care and were approved Animal Care and Use Committee of the Institute of Laboratory Animal Science of Peking Union Medical College (No.BL17001).

Isolation of ADSCs

To explore the effects of donor age on ADSCs, we randomly isolated ADSCs from a stromal-vascular cell fraction (SVF) derived from the abdominal subcutaneous adipose tissue of C57 mice. Adipose tissue was washed twice in phosphate buffer saline (PBS, Gibco, USA) and digested with 0.075% collagenase at a ratio 1:2 in 37℃water bath for 1h. Added fetal bovine serum (FBS, Gibco, USA) to neutralize them and centrifuged at 1500r/min for 11 min, then discarded the supernatant. Red blood cells lysed in Tris-NH4Cl at room temperature for 5min. And centrifuged at 1500r/min for 5 min after the suspension through 70μm filter, then discarded the supernatant. Lastly, cells seeded on 25cm2 tissue culture flasks in Dulbecco's modified Eagle's medium (DMEM, Gibco, USA) containing 10% FBS, 1% penicillin-streptomycin (Gibco, USA) and cultured in a humidified atmosphere at 37℃, 5% CO2. Medium was replaced every third day. When ~ 80% confluency was reached, cells were detached using 0.25% Trypsin-EDTA (Gibco, USA).

Morphology of ADSCs

ADSCs were observed by phase contrast microscope (Leica, German). And the ultrastructure was observed by transmission electron microscope (JEM-1400, Japan).

CCK-8 assay for growth curve

The growth curve of cell proliferation was drawn using CCK-8 kit (Beyotime,China). For this experiment, 100 microliters of 1,000 cells were added to ceach well of 96-well plate. Before test, add 10 microliters of CCK-8 solution directly to each well and continue incubation at 37℃, 5% CO2 for an hour. Determine the absorbance of light at 450nm wavelength. Finally, draw a growth curve according to the OD value.

Flow cytometry

ADSCs were harvested in the third passage (P3), washed in cold PBS, incubated with PE-conjugated hamster anti-mouse CD29 (HMb1-1, eBioscience), APC-conjugated rat anti-mouse CD105 (clone MJ7/18, Miltenyi Biotec), PE-Cyanin7-conjugated rat anti-mouse CD11b (M1/70, eBioscience), rat anti-mouse CD45 (clone 30F-11, BioLegend) for 30min from no light at 4℃. Cells acquisition was on a FACSAria IIIu cytometer (BD Biosciences). FlowJo (FlowJo LLC, Ashland, Oregon) software was used for data analysis.

Adipogenic and osteogenic differentiation

For adipogenesis, ADSCs were cultivated in 24-well culture dishes until 100% confluent. Regular culture medium was replaced with adipogenesis induction medium (Cyagen Biosciences, USA). Cells in control wells were cultivated in basic medium. Lipid droplets were detected after 14 days by Oil Red O staining. For osteogenesis, ADSCs seeded on 24-well plates were allowed to reach 70% confluency. Osteogenic differentiation was induced by adding osteogenic induction medium (Cyagen Biosciences, USA). Control

cells were cultivated in basic medium. After 21 days of cultivation, extracellular calcium accumulation was detected by Alizarin Red S.

Senescence-associated β-galactosidase(SA-β-gal) staining

To evaluate cellular senescence, ADSCs were fixed and stained with senescence-associated β-galactosidase (SA-β-Gal) staining kit (Beyotime, China) at 37℃ for 16 hours. The number of cells positively stained with β-Gal was calculated.

Cytokine array

A mouse cytokine array was used for simultaneous detection of 62 cytokines according to the manufacturer's protocol (Abcam, USA). Briefly, cell culture supernatant was added to the membrane of a mouse cytokine array. After washing the membrane, the detection antibody was applied and immunoblot images were captured using the BioSpectrum Imaging System. The intensity of each spot was measured using Image J software (version 2.0, Maryland, USA).

Next-generation RNA sequencing(RNAseq)

Sample collection and preparation

RNA quantification and qualification

RNA degradation and contamination was monitored on 1% agarose gels. RNA purity was checked using the NanoPhotometer® spectrophotometer (IMPLEN, CA, USA) .RNA concentration was measured using Qubit® RNA Assay Kit in Qubit® 2.0 Flurometer (Life Technologies, CA, USA).RNA integrity was assessed using the RNA Nano 6000 Assay Kit of the Bioanalyzer 2100 system (Agilent Technologies, CA, USA).

Library preparation for Transcriptome sequencing

A total amount of 3μg RNA per sample was used as input material for the RNA sample preparations. Sequencing libraries were generated using NEBNext® UltraTM RNA Library Prep Kit for Illumina® (NEB, USA) following manufacturer's recommendations and index codes were added to attribute sequences to each sample. At last, PCR products were purified (AMPure XP system) and library quality was assessed on the Agilent Bioanalyzer 2100 system.

Clustering and sequencing

The clustering of the index-coded samples was performed on a cBot Cluster Generation System using TruSeq PE Cluster Kit v3-cBot-HS (Illumia) according to the manufacturer's instructions. After cluster generation, the library preparations were sequenced on an Illumina Hiseq platform and 125 bp/150 bp paired-end reads were generated.

Data ananysis

Quality control

Raw data (raw reads) of fastq format were firstly processed through in-house perl scripts. In this step, clean data (clean reads) were obtained by removing reads containing adapter, reads containing ploy-N and low quality reads from raw data. At the same time, Q20, Q30 and GC content the clean data were calculated. All the downstream analyses were based on the clean data with high quality.

Quantification of gene expression level

HTSeq v0.6.0 was used to count the reads numbers mapped to each gene. And then FPKM of each gene was calculated based on the length of the gene and reads count mapped to this gene. FPKM, expected number of Fragments Per Kilobase of transcript sequence per Millions base pairs sequenced, considers the effect of sequencing depth and gene length for the reads count at the same time, and is currently the most commonly used method for estimating gene expression levels.

Differential expression analysis

Prior to differential gene expression analysis, for each sequenced library, the read counts were adjusted by edgeR program package through one scaling normalized factor. Differential expression analysis of two conditions was performed using the edgeR R package (3.12.1). The P values were adjusted using the Benjamini & Hochberg method. Corrected P-value of 0.05 and absolute foldchange of 2 were set as the threshold for significantly differential expression.

GO and KEGG enrichment analysis of differentially expressed genes

Gene Ontology (GO) enrichment analysis of differentially expressed genes was implemented by the clusterProfiler R package, in which gene length bias was corrected. GO terms with corrected P value less than 0.05 were considered significantly enriched by differential expressed genes.

KEGG is a database resource for understanding high-level functions and utilities of the biological system, such as the cell, the organism and the ecosystem, from molecular-level information, especially large-scale molecular datasets generated by genome sequencing and other high-through put experimental technologies (http://www.genome.jp/kegg/). We used clusterProfiler R package to test the statistical enrichment of differential expression genes in KEGG pathways.

GSEA and NTA of differentially expressed genes

Gene set enrichment analysis (GSEA) and network topology-based analysis (NTA) of differentially expressed genes was performed using the WEB-based Gene SeT AnaLysis Toolkit (http://www.broad.mit.edu/GSEA/)32. Parameters set as significance level at FDR < 0.05.

Quantitative RT-PCR

Gene expression in young, aged ADSCs was analyzed by quantitative real-time RT-PCR in technical triplicates using SYBR Green Premix Ex Taq II (Tli RNaseH Plus). Briefly, total RNA was extracted using Qiagen RNeasy Mini kit (Qiagen, Valencia, CA), following the manufacturer’ s protocols. cDNA was

synthesized using the cDNA archive reverse transcription kit (Life Technologies). Primers for Lcn2, Msr1, Tyrobp, Nfasc, Ccl12, Lef1, Mcpt1, Dthd1, Ajap1, Kcnmb4 were purchased from ThermoFisher. Actin was used as the reference gene for normalization. The cycle threshold (Ct) method of relative quantification of gene expression was used for these PCRs (ΔΔCt). The specific primers are listed in Supporting Information Table S1.

Statistical analysis

Mean and SE were calculated by averaging the results of three to six independent experiments performed with independent adipose cultures obtained from individual mouse for each experiment. SPSS software (version 25, Illinois, USA) was used for statistical analysis. P value < 0.05 was considered significant. ∗, p < 0.05.∗∗, p < 0.01. ∗∗∗, p < 0.001. ∗∗∗∗, p < 0.0001.

Results

Cellular senescence alters the morphology, cell proliferation and cytokines secreted by ADSCs

To assess cellular senescence in ADSCs, cell cultures from five 1-month-mice and five 20-month-mice in vitro cultivation. After 7 days, most cells adhered to the tissue culture plastic, assuming a fibroblast-like phenotype as flat and spindle shaped cells. Observed with phase-contract microscope, there were no morphological differences between the two donors (Fig. 1A). With increasing passage number, ADSCs had some senescence-associated changes: the increase of average cell size, flattening of cells, and accumulation of granular inclusions in cytoplasm.

ADSCs were fixed to further analyze its inner structure and cell composition. They presented large and round cell bodies with pseudopodia protruded. Homogeneous round lipid droplets and a lot of ribosomes were found in the cytoplasm. ADSCs have a relatively lobular or polygonal large nucleus and a high karyoplasmic ratio. In addition, there are abundant projections and depressions on the nuclear membrane and 1–3 nucleoli in the nucleus. In a further magnification view, the mitochondrion in the cytoplasm had a bilayer membrane structure with an inner membrane folded into cristae. Compared with ADSCs from 1-month mice (1M ADSCs), ADSCs from 20-month mice (20M ADSCs) showed swollen rough endoplasmic reticulum, a large number of medullary corpuscles in cytoplasm (Fig. 1B, B6) and lipid droplets increased (Fig. 1B, B7). Mitochondrion was swollen with altered crest structure (Fig. 1B, B8).

To further investigate whether ADSCs from aged donors are functional, the differentiation capacity of 1M and 20M ADSCs into the adipogenic, osteogenic lineages was analysed. The results confirmed that the 20M ADSCs still have the two lineages differention ability as 1M ADSCs (Fig. 1C, D and E). In addition, the functionality of cytokines secreting was examined by employing a cytokine array. As shown in Fig. 1G, the levels of chemokines in cell culture supernatant were obviously increased with age, including granulocyte-macrophage colony-stimulating factor (GM-CSF), interleukin-4 (IL-4), IL-13, IL-17,

macrophage inflammatory protein-1α (MIP-1α) or C-C motif chemokine ligand 3 (CCL3) and thymus-expressed chemokine (TECK) or CCL25.

When cultured to P3, cells were seeded in 24-well plate at a density of 1×10^3 per well, and measured every day to draw the growth curve of ADSCs from 1M and 20M mice. As shown in Fig. 1F, the young ADSCs entered exponential growth period in a shorter time and grew in a fast speed compared to the aged.

A ADSCs morphology under optical microscope. Scale bars of 10× groups, 100μm. Scale bars of 20× groups, 75μm. **B** Ultrastructural changes of ADSCs under transmission electron microscope(TEM). B1-B4 represent ADSCs from 1-month (1M) mice while B5-B8 represent 20-month(20M). **C** Osteogenic differentiation differences of ADSCs from 1M and 20M mice. Scale bars, 100μm **D, E** Adipogenicity differences and quantitative analysis of ADSCs from 1M and 20M mice. Scale bars, 100μm **F** Growth curve of ADSCs. **G** Cytokine assay of ADSCs from 1M and 20M donors. $*$, $p < 0.05$.

An elevated number of apoptotic cells accompanied by an increase of cells in the quiescent G0 phase from 20M mice

All the cells matched the ADSCs markers——positive in CD29, CD105 and negative in CD45, CD11b. As the Fig. 2A showed, the average percentage of CD29, CD105, CD45, CD11b in 1M ADSCs is 96.9, 28.5, 25.0, 11.8, while the average percentage in 20M ADSCs is 97.2, 42.0, 19.1, 4.7. 1M and 20M cells have no significant difference in these surface markers, which means the adipose tissue obtained from young mice has the same yield of the old under a same condition.

SA–β-Gal staining indicated few senescence cells at early passages among the two types of ADSCs (Fig. 2B). After two serial cell passages every 3–4 days, the number of SA–β-Gal-positive cells was determined, and the two groups have no significant difference (Fig. 2B and E). The senescent cells number was increased as the passage number increased, indicating that passage time has a greater effect on senescence than donor age.

The influence of donor age on the cell cycle and apoptosis was measured by flow cytometry (Fig. 2C, D, G, and H). An increase in apoptotic cells was detected in 20M ADSCs compared with 1M ADSCs (Fig. 2C and G). 20M Cells in G0 phase increase and cells in G1 and S/G2/M phases decrease were noted compared with 1M ADSCs (Fig. 2D and H).

Finally, analysis of aging-related genes expression, using qRT-PCR, respectively, demonstrated a drastic increase expression of p19 in 20M ADSCs, compared to 1M cells. p16 and p21 are two markers frequently associated with cellular senescence[33], both of which were highly expressed in cells isolated from the old donors (Fig. 2F).

A The proportion of ADSCs expressing positive and negative surface marker. **B, E** SA-β-gal staining and quantitative analysis of 1M and 20M ADSCs. Scale bars, 100μm. **C, D, G, and H** Flow cytometry and

quantitative analysis of Annexin V and 7-AAD between 1M and 20M ADSCs. ∗, $p < 0.05$. ∗∗, $p < 0.01$. **F** Age-related gene expression of 1M and 20M ADSCs. ∗∗, $p < 0.01$. ∗∗∗∗, $p < 0.0001$.

Lef1 and Ddx3y were the specific elements for the down-regulated and up-regulated genes, respectively, in mADSCs with age.

To explore the underlying mechanism, we performed RNA-seq on ADSCs from 1M and 20M mice. Sequencing yielded on average 39.2 million raw reads per 1M ADSCs and 33.5 million raw reads per 20M ADSCs. As shown in Supporting Information Table S2, the Q20 of 1M ADSCs and 20M ADSCs were more than 95%, and the Q30 were more than 90%. Alignment analysis resulted in an average total read mapping rate of 95.51% and a proper pair alignment rate of 88.35% in 1M ADSCs, while 20M's average total read mapping rate was 95.39% and a proper pair alignment rate was 88.26%. The results were listed as Supporting Information Table S3. The RPKM value of two groups were listed in Supporting Information Table S4. It is commonly supposed to be a marker of significant difference in gene expression when it's more than 1.

1M and 20M ADSCs have 11,041 genes in common (Fig. 3A). The overall distribution of differentially expressed genes (DEGs) between the two groups were selected according to the value of fold change and the significance level, which could be inferred completely in volcano plot. DEGs from 20M mice compared to that of the 1M mice were colored with green and red, regarding 431 significantly down-regulated and 1,481 significantly up-regulated genes, respectively (Fig. 3C). Top 10 of the most down-regulated genes were *Lef1, Lingo2, Gpbar1, Mcpt1, Hecw1, Dthd1, Gpr149, Ajap1, Zfp82, Fibcd1* and top 10 of the most up-regulated genes were *Ddx3y, S100a9, S100a8, Eif2s3y, Ngp, Chil3, Ltf, Saa3, Kdm5d and Uty* according to the absolute value of $\log_2$Foldchange with age (Fig. 3D). The DEGs were verified by qRT-PCR, and the gene expression pattern was consistent with the transcriptome results(Fig. 3B).

A Venn chart showing 11041 differentially expressed genes (DEGs) in common between 1M and 20M ADSCs. Corrected P-value of 0.05 and absolute fold change of 2 were set as the threshold for significantly differential expression. **B** Verification of DEGs through qRT-PCR. ∗, $p < 0.05$. ∗∗, $p < 0.01$∗, $p < 0.0001$. **C** Volcano plot showing DEGs significantly down-regulated (Green) and up-regulated (Red) compared to 1M ADSCs. **D** Top 10 of DEGs profiles. Green bar indicates significantly down-regulated DEGs, while red indicates significantly up-regulated DEGs.

Chemokine signaling pathway and Hippo signaling pathway were the top potential signaling pathways, indicating that these two pathways related to age-related alterations in mADSCs.

To explore the changing profile of gene expression level, up-regulated and down-regulated genes were analyzed separately. The DEGs were grouped in three GO categories: Biological Process(BP), Cellular Component(CC) and Molecular Function(MF). The up-regulated DEGs were mostly associated with innate immune response, inflammatory response, leukocyte migration, leukocyte chemotaxis, cell chemotaxis in BP. As for CC, the genes are mostly expressed differentially in contractile fiber, myofiril. Cytokine activity, chemokine activity are the mostly related terms of differentially expressed genes in MF (Fig. 4A). KEGG is

a database resource for understanding high-level functions and utilities of the biological system, such as the cell, the organism and the ecosystem, from molecular-level information, especially large-scale molecular datasets generated by genome sequencing and other high-throughput experimental technologies[34]. KEGG analysis further identified the cytokine-cytokine receptor interaction and chemokine signaling pathway as the top scoring pathway among the age-related up-regulated genes (Fig. 4C).

GO and KEGG pathway enrichment of age-related down-regulated DEGs were showed in Fig. 4B and D. The results of GO showed that DEGs were enriched in axon devilment, mesenchymal cell development in BP, and growth factor activity in MF (Fig. 4B). Seven KEGG pathway were significantly enriched, namely gastric cancer, Hippo signaling pathway, vascular smooth muscle contraction, mircoRNAs in cancer, axon guidance, TGF-beta signaling pathway, and dilated cardiomyopathy (DCM). Gastric cancer, Hippo signaling pathway and axon guidance were the highest ratio of the number of DEGs annotated to corresponding pathway to the number of annotated DEGs i.e., 11 out of 124 genes in response to aging (Fig. 4D).

A, B GO enrichment of age-related DEGs. The top ten terms enriched for each category were listed. **A** Up-regulated genes enrichment; **B** Down-regulated genes enrichment. **C, D** KEGG pathway enrichment of age-related DEGs. The top twenty pathways enriched were listed. Count, differential gene count in indicated pathway; padj, adjusted P value of indicated pathway. **C** Up-regulated genes enrichment; **D** Down-regulated genes enrichment.

Chemokine signaling pathway was the crucial signaling pathway in mADSCs with age.

We further performed GO and KEGG pathway enrichment analysis on all genes we enriched. The functional categorization revealed that most of the DEGs with age function in inflammatory response, contractile fiber, and calcium ion binding(Table 1). Overall DEGs were found to be associated with the following signaling pathways: Chemokine, Calcium, Rap1, PI3K-Akt, MAPK and cGMP-PKG (Fig. 5A).

To further investigate the involved signaling pathway from an overall perspective, a gene set analysis was conducted in significance level at FDR < 0.05. Based on the parameters, 49 positive related categories and 1 negative related categories are identified as enriched categories, in which 5 most significant categories and representatives in the reduced sets are shown in Fig. 5B. Clustering analysis showed that chemokine signaling pathway clustered with the highest normalized enrichment score (NES,1.8068) while the NES of negative related one DNA replication was − 1.7139. Enriched genes were shown in red in the map of chemokine signaling pathway (Fig. 5C, Supporting Information Table S5). Meanwhile, screened differential genes were imported into the PANTHER tool for pathway enrichment analysis. Inflammation mediated by chemokine and cytokine signaling pathway was the most significant positive category (Supporting Information Fig.S1).

Table 1
GO functional annotation of overall DEGs

Category	GO ID	Description	GeneRatio[a]	Padj[b]	Up[c]	Down[d]
BP	GO:0006954	inflammatory response	144/1636	1.08E-26	130	14
	GO:0045087	innate immune response	135/1636	1.62E-25	126	9
	GO:0003012	muscle system process	103/1636	2.47E-23	86	17
	GO:0006935	chemotaxis	123/1636	2.47E-23	100	23
	GO:0050900	leukocyte migration	89/1636	2.47E-23	83	6
CC	GO:0043292	contractile fiber	82/1676	5.36E-26	66	16
	GO:0030016	myofibril	75/1676	2.13E-23	62	13
	GO:0044449	contractile fiber part	73/1676	2.78E-23	58	15
	GO:0030017	sarcomere	68/1676	4.63E-22	55	13
	GO:0009897	external side of plasma membrane	77/1676	1.09E-18	68	9
MF	GO:0005509	calcium ion binding	112/1622	1.43E-12	89	23
	GO:0008009	chemokine activity	18/1622	5.38E-09	16	2
	GO:0005125	cytokine activity	41/1622	1.92E-08	36	5
	GO:0030414	peptidase inhibitor activity	39/1622	4.59E-08	33	6
	GO:0005126	cytokine receptor binding	54/1622	5.04E-08	46	8

Abbreviations: GeneRatio, differential gene count in indicated pathway versus total differential gene count; Padj, adjusted P value of indicated pathway; Up, up-regulated differential gene count in indicated pathway; Down, down-regulated differential gene count in indicated pathway.

A KEGG pathway enrichment of age-related DEGs. **B** Volcano and enrichment plot of GSEA in significance level at FDR < 0.05. NES, normalized enrichment score. FDR, false discovery rate. **C** Map of chemokine signaling pathway in KEGG database. Mapped DEGs were shown in red.

The CCL7-CCL2-CCR2 axis regulates age-related changes in mADSCs.

During the evaluation of the clusters enriched in chemokine signaling pathway for Biogrid data, it was found that the Biogrid PPI network had one node CCL2 of very high degree corresponding to the chemokine. Enrichment analysis showed total number of 18 genes in the expanded sub-network, and top 5 neighbors based on the probability of random walk method was listed in Supporting Information Table S5. All seeds and top ranking neighbors in the expanded sub-network can enrich to 5 GO BP categories (Fig. 6A and B). Results showed total number of 3 genes, CCL7, CCL2, CCR2 in the retrieved sub-network, which enrich to 5 GO BP categories (Fig. 6C and D).

A Expanded PPI network of DEGs mapped chemokine signaling pathway. **B** Top 5 of GO BP categories that all seeds and top ranking neighbors in A could be enriched. **C** Retrieved PPI network of DEGs mapped chemokine signaling pathway. **D** Top 5 of GO BP categories that *Ccl7, Ccl2, Ccr2* could be enriched.

Discussion

Herein, we describe age-related changes in ADSCs from 1-month and 20-month mice to clear up the consistency of ADSCs senescence and organismal aging, and consider its possible mechanisms, according to the results of transcriptome analysis.

In this study, the abdominal subcutaneous adipose tissue was chosen because it is the most commonly used source of ADSCs that is relatively easy to acquire and large quantities of adipose cells are obtained through liposuction[35,36]. Then we detected the morphology, ultrastructure, proliferation, differentiation, function of secreting cytokines, surface markers, apoptosis, cell cycle, SA-β-gal staining, and gene expression of ADSCs from these two age groups. Ultrastructures showed that ADSCs from 20-month mice had some senescence-associated changes, like increased lipid droplets. The growth curve presented that 20M ADSCs had less ability to proliferation than 1M ADSCs. At present, the identification of senescent cells relies on a combination of multiple markers. Di Micco et al have summarized senescence biomarkers based on previous published researches, like accumulation of p21 and p16[37], in which p16 is the best-characterized marker of senescence[38]. In accordance with this, 20M ADSCs expressed higher levels of p16, p19, p21 compared to 1M ADSCs, indicating the PI3K/Akt pathway is activated[39], which is consistent with our KEGG pathway enrichment.

Cellular senescence was also defined as a state of irreversible cell cycle arrest[40]. The flow cytometry assay further verified that ADSCs from 20-month mice were more significantly arrested at the G0 phase with more apoptosis cells than 1-month mice. In short, we found that ADSCs from aged groups had some senescence-associated changes in ultrastructure, proliferation, gene expression, and cell cycle.

So could we conclude that senescence of individuals is consistent with that of ADSCs? Maybe not. We took it a step further and explored more senescent parameters of ADSCs from aged donors. SA-β-gal was the first and the most widely used biomarkers of senescence while SA-β-gal-positive cells have increased cell size which senescent cells have increased cell size[41,42]. In our observation, primary ADSCs did not express SA-β-gal and have the normal morphology, whether obtained from 1-month or 20-month mice, while SA-β-gal increased with flat morphology after serial passaging. Components of the senescence-associated secretory phenotype (SASP), mainly the proinflammatory cytokines IL-6, which not increased in culture supernatant of 20M ADSCs compared to 1M ADSCs, indicating that senescence phenotypes are highly heterogeneous and may differ depending on the cell type. The cytokine array showed that increased GM-CSF, IL-4, IL-13, IL-17, CCL3, and CCL25 could be SASP profiles for senescent ADSCs. Importantly, no differences shown in terms of their surface markers and differentiation capacity.

Then, what molecular mechanisms are responsible for these phenotypes? Previously, a few age-related key pathways have emerged, like insulin and IGF-1 signaling, and its multiple targets are the FOXO family of transcription factors and the PI3K/Akt/mTOR, which are also involved in aging[43–45]. In a recent report, the single-cell transcriptomic analysis of ADSCs from old donors was conducted several enriched pathways including CXCR4 signaling and concluded that *p16, IL-6, and Cxcl1* would be helpful for understanding the biology of senescence[46].

Our RNA-seq analysis revealed that some transcriptome changes affecting genes involved in age-related variations, like *Lef1, Lingo2, Dxd3y*. One of the major differences may stem from the up-regulated genes because of the quantity gap. DEGs are significantly associated with inflammatory response, chemotaxis, chemokine activity, and chemokine, MAPK, PI3K-Akt signaling pathways. Hippo signaling pathway and biological processes are also associated with aging, such as anti-aging pathways AMP-activated protein kinase (AMPK) and sirtuin (SIRT)[47], which the down-regulated DEGs compared to 1M ADSCs was enriched in our analysis. Besides, whether KEGG enrichment analysis or GSEA, the expression levels of genes related to the chemokine signaling pathway were found to be altered. Moreover, our bioinformatic gene network analysis of chemokine-related DEGs showed their association with CCL7-CCL2-CCR2 axis.

Conclusion

The aim of this work was to furthermore know the characteristics of ADSCs from old donors and verify the influence of senescence on the proliferation and differentiation of ADSCs in vitro, providing the theoretical basis for the clinical application of autologous ADSCs transplantation. ADSCs from old donors showed some changes as natural aging. Moreover, ADSCs can stand long-term cryopreservation with a high survival rate after resuscitation without significant influence on the proliferation and differentiation ability[48,49]. Therefore, we suggest that ADSCs should be cryopreserved in youth with minimum number of passages, so as to make autologous transplantation work better for senile diseases. Furthermore, our findings reveal CCL7-CCL2-CCR2, a novel aging-associated regulatory axis, as a potential target for gene therapy to alleviate senescence in ADSCs.

Abbreviations

ADSCs: Adipose-derived stem cells; RNA-seq: Transcriptome sequencing; SA-β-gal: Senescence-associated β-galactosidase; SASP: Senescence-associated secretory phenotype; DEGs: Differentially expressed genes; NES: Normalized enrichment score.

Declarations

Ethics approval and consent to participate Not applicable.

Availability of data and materials All relevant data are within the paper and its online supplementary information files.

Competing interests None declared.

Funding The authors acknowledge the financial support from the National Key Research and Development Project of China (2017YFA0105200), Natural Science Foundation of Beijing Municipality(5202024), and CAMS Innovation Fund for Medical Sciences(2016-I2M-1-012).

Authors' contributions KYL, GYS, XPL completed the experiments. KYL, XYL and YYH performed the analysis of RNA-seq. KYL wrote the manuscript. LB and CQ designed and supervised the project. All the authors read and approved the manuscript.

Acknowledgements None declared.

References

1. Kirkwood TBL. Understanding the odd science of aging. Cell. 2005;120(4):437–47. (In eng).
2. Wagner K-H, Cameron-Smith D, Wessner B, Franzke B. Biomarkers of Aging: From Function to Molecular Biology. Nutrients 2016;8(6) (In eng). DOI:10.3390/nu8060338.
3. Boland B, Yu WH, Corti O, et al. Promoting the clearance of neurotoxic proteins in neurodegenerative disorders of ageing. Nature reviews Drug discovery. 2018;17(9):660–88. DOI:10.1038/nrd.2018.109. (In eng).
4. Chan T-M, Chen JY-R, Ho L-I, et al. ADSC therapy in neurodegenerative disorders. Cell Transplant. 2014;23(4–5):549–57. DOI:10.3727/096368914X678445. (In eng).
5. Cook G, Iacobelli S, van Biezen A, et al. High-dose therapy and autologous stem cell transplantation in patients with POEMS syndrome: a retrospective study of the Plasma Cell Disorder sub-committee of the Chronic Malignancy Working Party of the European Society for Blood & Marrow Transplantation. Haematologica. 2017;102(1):160–7. DOI:10.3324/haematol.2016.148460. (In eng).
6. Venkataramana NK, Kumar SKV, Balaraju S, et al. Open-labeled study of unilateral autologous bone-marrow-derived mesenchymal stem cell transplantation in Parkinson's disease. Translational

research: the journal of laboratory clinical medicine. 2010;155(2):62–70. DOI:10.1016/j.trsl.2009.07.006. (In eng).

7. Martinez HR, Gonzalez-Garza MT, Moreno-Cuevas JE, Caro E, Gutierrez-Jimenez E, Segura JJ. Stem-cell transplantation into the frontal motor cortex in amyotrophic lateral sclerosis patients. Cytotherapy. 2009;11(1):26–34. DOI:10.1080/14653240802644651. (In eng).
8. Blanquer M, Moraleda JM, Iniesta F, et al. Neurotrophic bone marrow cellular nests prevent spinal motoneuron degeneration in amyotrophic lateral sclerosis patients: a pilot safety study. Stem Cells. 2012;30(6):1277–85. DOI:10.1002/stem.1080. (In eng).
9. Gurusamy N, Alsayari A, Rajasingh S, Rajasingh J. Adult Stem Cells for Regenerative Therapy. Progress in molecular biology and translational science 2018;160 (In eng). DOI: 10.1016/bs.pmbts.2018.07.009.
10. Zuk PA, Zhu M, Ashjian P, et al. Human adipose tissue is a source of multipotent stem cells. Molecular biology of the cell. 2002;13(12):4279–95. (In eng).
11. Zuk PA, Zhu M, Mizuno H, et al. Multilineage cells from human adipose tissue: implications for cell-based therapies. Tissue engineering. 2001;7(2):211–28. (In eng).
12. Planat-Benard V, Silvestre J-S, Cousin B, et al. Plasticity of human adipose lineage cells toward endothelial cells: physiological and therapeutic perspectives. Circulation. 2004;109(5):656–63. (In eng).
13. Yokoyama R, Ii M, Masuda M, et al. Cardiac Regeneration by Statin-Polymer Nanoparticle-Loaded Adipose-Derived Stem Cell Therapy in Myocardial Infarction. Stem cells translational medicine. 2019;8(10):1055–67. DOI:10.1002/sctm.18-0244. (In eng).
14. Wystrychowski W, Patlolla B, Zhuge Y, Neofytou E, Robbins RC, Beygui RE. Multipotency and cardiomyogenic potential of human adipose-derived stem cells from epicardium, pericardium, and omentum. Stem Cell Res Ther. 2016;7(1):84. DOI:10.1186/s13287-016-0343-y. (In eng).
15. Qin Y, Zhou C, Wang N, Yang H, Gao W-Q. Conversion of Adipose Tissue-Derived Mesenchymal Stem Cells to Neural Stem Cell-Like Cells by a Single Transcription Factor, Sox2. Cellular reprogramming. 2015;17(3):221–6. DOI:10.1089/cell.2015.0001. (In eng).
16. Takahashi H, Ishikawa H, Tanaka A. Regenerative medicine for Parkinson's disease using differentiated nerve cells derived from human buccal fat pad stem cells. Hum Cell. 2017;30(2):60–71. DOI:10.1007/s13577-017-0160-3.
17. McCoy MK, Martinez TN, Ruhn KA, et al. Autologous transplants of Adipose-Derived Adult Stromal (ADAS) cells afford dopaminergic neuroprotection in a model of Parkinson's disease. Exp Neurol. 2008;210(1):14–29. DOI:10.1016/j.expneurol.2007.10.011.
18. García-Honduvilla N, Cifuentes A, Ortega MA, et al. High Sensitivity of Human Adipose Stem Cells to Differentiate into Myofibroblasts in the Presence of Egg Extract. Stem cells international 2017;2017:9142493. (In eng). DOI: 10.1155/2017/9142493.
19. Fang Z, Yang Q, Xiong W, et al. Effect of CGRP-adenoviral vector transduction on the osteoblastic differentiation of rat adipose-derived stem cells. PloS one. 2013;8(8):e72738.

DOI:10.1371/journal.pone.0072738. (In eng).

20. Perdisa F, Gostyńska N, Roffi A, Filardo G, Marcacci M, Kon E. Adipose-Derived Mesenchymal Stem Cells for the Treatment of Articular Cartilage: A Systematic Review on Preclinical and Clinical Evidence. Stem cells international 2015;2015:597652. (In eng). DOI: 10.1155/2015/597652.
21. Tabatabaei Qomi R, Sheykhhasan M. Adipose-derived stromal cell in regenerative medicine: A review. World journal of stem cells. 2017;9(8):107–17. DOI:10.4252/wjsc.v9.i8.107. (In eng).
22. Gonzalez-Garza MT, Cruz-Vega DE. Regenerative capacity of autologous stem cell transplantation in elderly: a report of biomedical outcomes. Regenerative medicine. 2017;12(2):169–78. DOI:10.2217/rme-2016-0038. (In eng).
23. Schwerk A, Altschuler J, Roch M, et al. Adipose-derived human mesenchymal stem cells induce long-term neurogenic and anti-inflammatory effects and improve cognitive but not motor performance in a rat model of Parkinson's disease. Regenerative Medicine 2015;10(4):431 – 46. (Research Support, Non-U.S. Gov't).
24. Berg J, Roch M, Altschuler J, et al. Human adipose-derived mesenchymal stem cells improve motor functions and are neuroprotective in the 6-hydroxydopamine-rat model for Parkinson's disease when cultured in monolayer cultures but suppress hippocampal neurogenesis and hippocampal memory function when cultured in spheroids. Stem Cell Reviews Reports. 2015;11(1):133–49. (Research Support, Non-U.S. Gov't).
25. Schultz MB, Sinclair DA. When stem cells grow old: phenotypes and mechanisms of stem cell aging. Development 2016;143(1) (In eng). DOI:10.1242/dev.130633.
26. Schipper BM, Marra KG, Zhang W, Donnenberg AD, Rubin JP. Regional anatomic and age effects on cell function of human adipose-derived stem cells. Ann Plast Surg. 2008;60(5):538–44. DOI:10.1097/SAP.0b013e3181723bbe. (In eng).
27. Alt EU, Senst C, Murthy SN, et al. Aging alters tissue resident mesenchymal stem cell properties. Stem cell research. 2012;8(2):215–25. DOI:10.1016/j.scr.2011.11.002. (In eng).
28. Shi Y, Niedzinski JR, Samaniego A, Bogdansky S, Atkinson BL. Adipose-derived stem cells combined with a demineralized cancellous bone substrate for bone regeneration. Tissue engineering Part A. 2012;18(13–14):1313–21. DOI:10.1089/ten.TEA.2011.0357. (In eng).
29. Zhu M, Kohan E, Bradley J, Hedrick M, Benhaim P, Zuk P. The effect of age on osteogenic, adipogenic and proliferative potential of female adipose-derived stem cells. J Tissue Eng Regen Med. 2009;3(4):290–301. DOI:10.1002/term.165. (In eng).
30. Aust L, Devlin B, Foster SJ, et al. Yield of human adipose-derived adult stem cells from liposuction aspirates. Cytotherapy 2004;6(1) (In eng).
31. Mojallal A, Lequeux C, Shipkov C, et al. Influence of age and body mass index on the yield and proliferation capacity of adipose-derived stem cells. Aesthetic Plast Surg. 2011;35(6):1097–105. DOI:10.1007/s00266-011-9743-7. (In eng).
32. Liao Y, Wang J, Jaehnig EJ, Shi Z, Zhang B. WebGestalt 2019: gene set analysis toolkit with revamped UIs and APIs. Nucleic Acids Res. 2019;47(W1):W199-w205. DOI:10.1093/nar/gkz401. (In

eng).

33. Campisi J. d'Adda di Fagagna F. Cellular senescence: when bad things happen to good cells. Nature reviews Molecular cell biology. 2007;8(9):729–40. (In eng).
34. Kanehisa M, Furumichi M, Tanabe M, Sato Y, Morishima K. KEGG: new perspectives on genomes, pathways, diseases and drugs. Nucleic Acids Res. 2017;45(D1):D353-d361. DOI:10.1093/nar/gkw1092. (In eng).
35. Li H, Zhu L, Chen H, et al. Generation of Functional Hepatocytes from Human Adipose-Derived MYC KLF4 GMNN Stem Cells Analyzed by Single-Cell RNA-Seq Profiling. Stem cells translational medicine 2018;7(11):792–805. (In eng). DOI: 10.1002/sctm.17-0273.
36. Zhou W, Lin J, Zhao K, et al. Single-Cell Profiles and Clinically Useful Properties of Human Mesenchymal Stem Cells of Adipose and Bone Marrow Origin. Am J Sports Med. 2019;47(7):1722–33. DOI:10.1177/0363546519848678. (In eng).
37. Di Micco R, Krizhanovsky V, Baker D. d'Adda di Fagagna F. Cellular senescence in ageing: from mechanisms to therapeutic opportunities. Nat Rev Mol Cell Biol. 2021;22(2):75–95. DOI:10.1038/s41580-020-00314-w. (In eng).
38. Grosse L, Wagner N, Emelyanov A, et al. Defined p16 Senescent Cell Types Are Indispensable for Mouse Healthspan. Cell Metabol 2020;32(1) (In eng). DOI:10.1016/j.cmet.2020.05.002.
39. Yu K-R, Kang K-S. Aging-related genes in mesenchymal stem cells: a mini-review. Gerontology. 2013;59(6):557–63. DOI:10.1159/000353857. (In eng).
40. Zhou X, Hong Y, Zhang H, Li X. Mesenchymal Stem Cell Senescence and Rejuvenation: Current Status and Challenges. Frontiers in cell developmental biology. 2020;8:364. DOI:10.3389/fcell.2020.00364. (In eng).
41. Dimri GP, Lee X, Basile G, et al. A biomarker that identifies senescent human cells in culture and in aging skin in vivo. Proc Natl Acad Sci U S A. 1995;92(20):9363–7. DOI:10.1073/pnas.92.20.9363. (In eng).
42. Biran A, Zada L, Abou Karam P, et al. Quantitative identification of senescent cells in aging and disease. Aging Cell. 2017;16(4):661–71. DOI:10.1111/acel.12592. (In eng).
43. Campisi J, Kapahi P, Lithgow GJ, Melov S, Newman JC, Verdin E. From discoveries in ageing research to therapeutics for healthy ageing. Nature. 2019;571(7764):183–92. DOI:10.1038/s41586-019-1365-2. (In eng).
44. Ogg S, Paradis S, Gottlieb S, et al. The Fork head transcription factor DAF-16 transduces insulin-like metabolic and longevity signals in C. elegans. Nature. 1997;389(6654):994–9. DOI:10.1038/40194. (In eng).
45. López-Otín C, Blasco MA, Partridge L, Serrano M, Kroemer G. The hallmarks of aging. Cell. 2013;153(6):1194–217. DOI:10.1016/j.cell.2013.05.039. (In eng).
46. Wang B, Liu Z, Chen VP, et al. Transplanting cells from old but not young donors causes physical dysfunction in older recipients. Aging Cell. 2020;19(3):e13106. DOI:10.1111/acel.13106. (In eng).

47. Yeung YT, Guerrero-Castilla A, Cano M, Muñoz MF, Ayala A, Argüelles S. Dysregulation of the Hippo pathway signaling in aging and cancer. Pharmacol Res. 2019;143:151–65. DOI:10.1016/j.phrs.2019.03.018. (In eng).
48. Durandt C, Dessels C, da Silva C, Murdoch C, Pepper MS. The Effect of Early Rounds of ex vivo Expansion and Cryopreservation on the Adipogenic Differentiation Capacity of Adipose-Derived Stromal/Stem Cells. Sci Rep. 2019;9(1):15943. DOI:10.1038/s41598-019-52086-9. (In eng).
49. Kumar A, Xu Y, Yang E, Wang Y, Du Y. Fidelity of long-term cryopreserved adipose-derived stem cells for differentiation into cells of ocular and other lineages. Exp Eye Res. 2019;189:107860. DOI:10.1016/j.exer.2019.107860. (In eng).

Figures

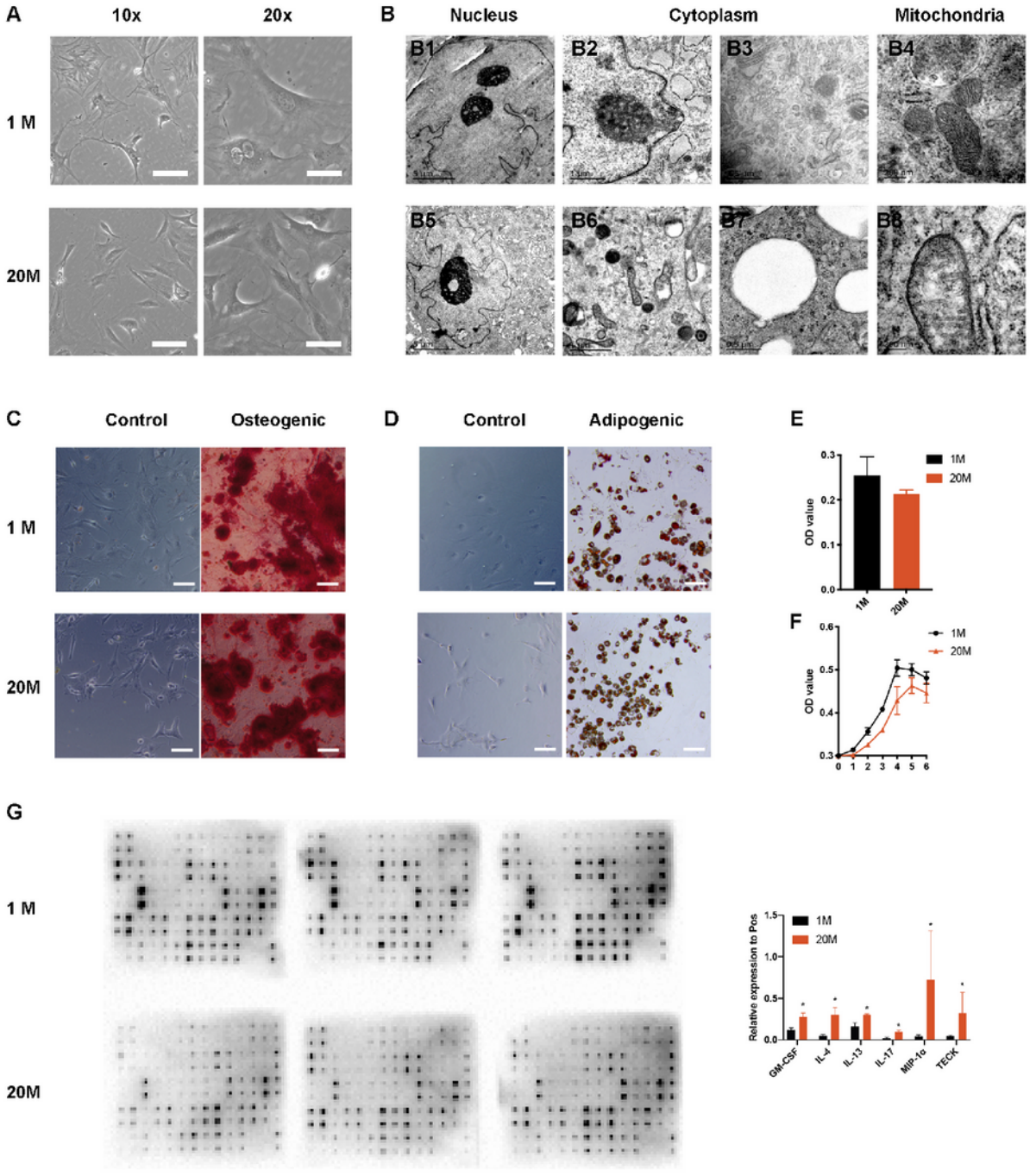

Figure 1

Morphology and functions of ADSCs from 1M and 20M mice A ADSCs morphology under optical microscope. Scale bars of 10× groups, 100μm. Scale bars of 20× groups, 75μm. B Ultrastructural changes of ADSCs under transmission electron microscope(TEM). B1-B4 represent ADSCs from 1-month (1M) mice while B5-B8 represent 20-month(20M). C Osteogenic differentiation differences of ADSCs from 1M and 20M mice. Scale bars, 100μm D, E Adipogenicity differences and quantitative analysis of ADSCs

from 1M and 20M mice. Scale bars, 100μm F Growth curve of ADSCs. G Cytokine assay of ADSCs from 1M and 20M donors. ∗, p < 0.05.

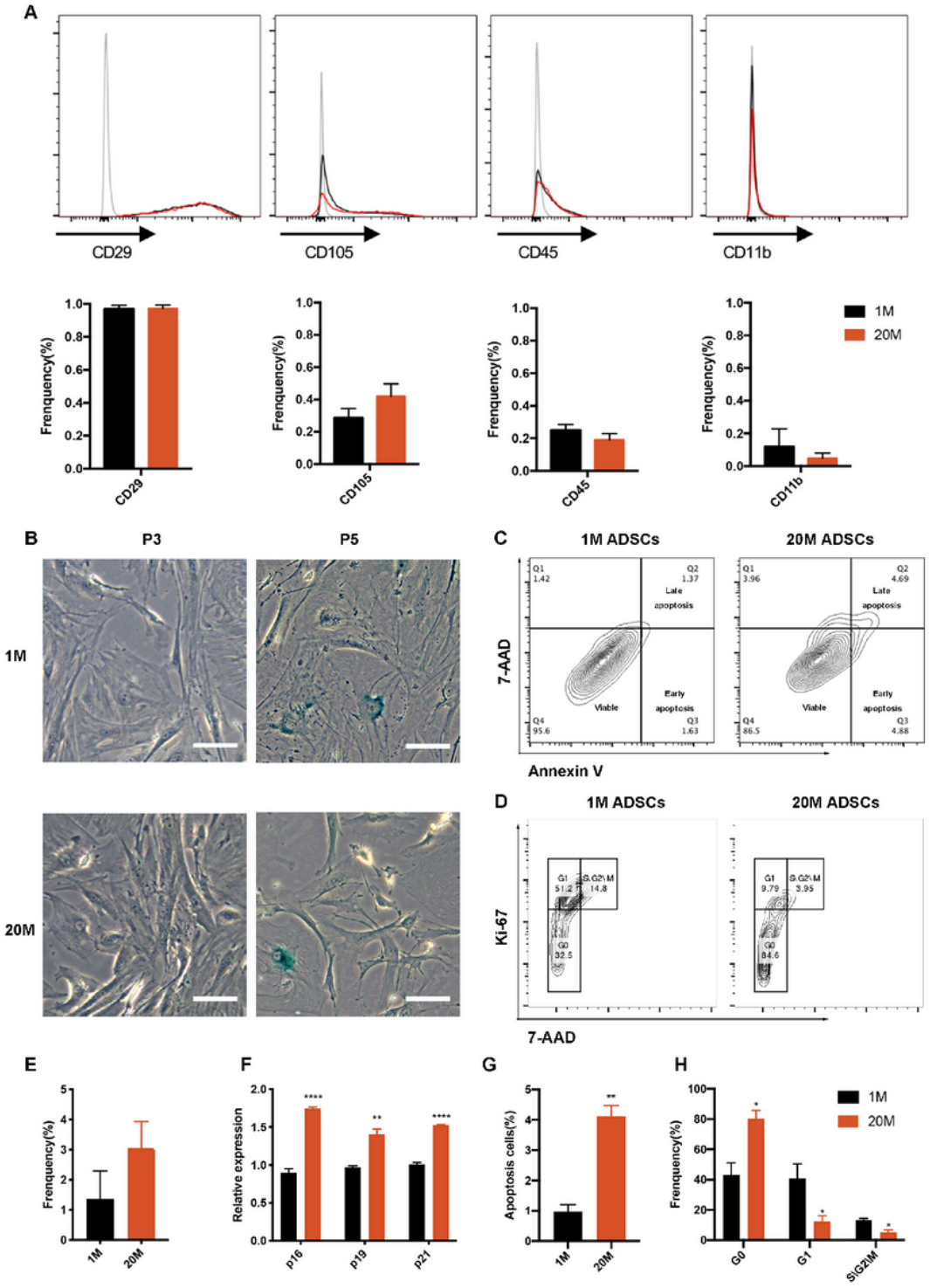

Figure 2

Surface markers and age-related phenotypes of ADSCs A The proportion of ADSCs expressing positive and negative surface marker. B, E SA-β-gal staining and quantitative analysis of 1M and 20M ADSCs. Scale bars, 100μm. C, D, G, and H Flow cytometry and quantitative analysis of Annexin V and 7-AAD

between 1M and 20M ADSCs. ∗, p < 0.05. ∗∗, p < 0.01. F Age-related gene expression of 1M and 20M ADSCs. ∗∗, p < 0.01. ∗∗∗∗, p < 0.0001.

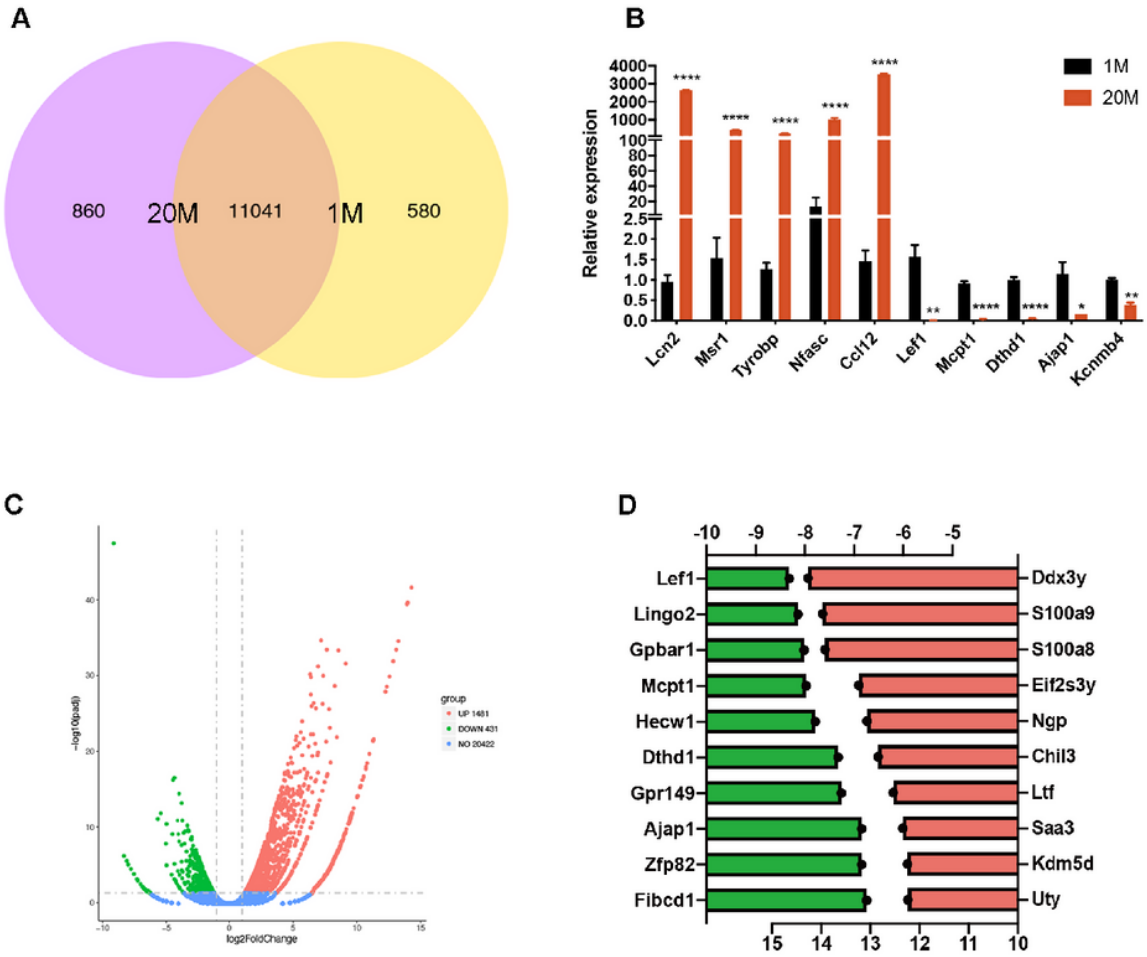

Figure 3

Differential Gene Expression Analysis (DGA) A Venn chart showing 11041 differentially expressed genes (DEGs) in common between 1M and 20M ADSCs. Corrected P-value of 0.05 and absolute fold change of 2 were set as the threshold for significantly differential expression. B Verification of DEGs through qRT-PCR. ∗, p < 0.05. ∗∗, p < 0.01∗, p < 0.0001. C Volcano plot showing DEGs significantly down-regulated (Green) and up-regulated (Red) compared to 1M ADSCs. D Top 10 of DEGs profiles. Green bar indicates significantly down-regulated DEGs, while red indicates significantly up-regulated DEGs.

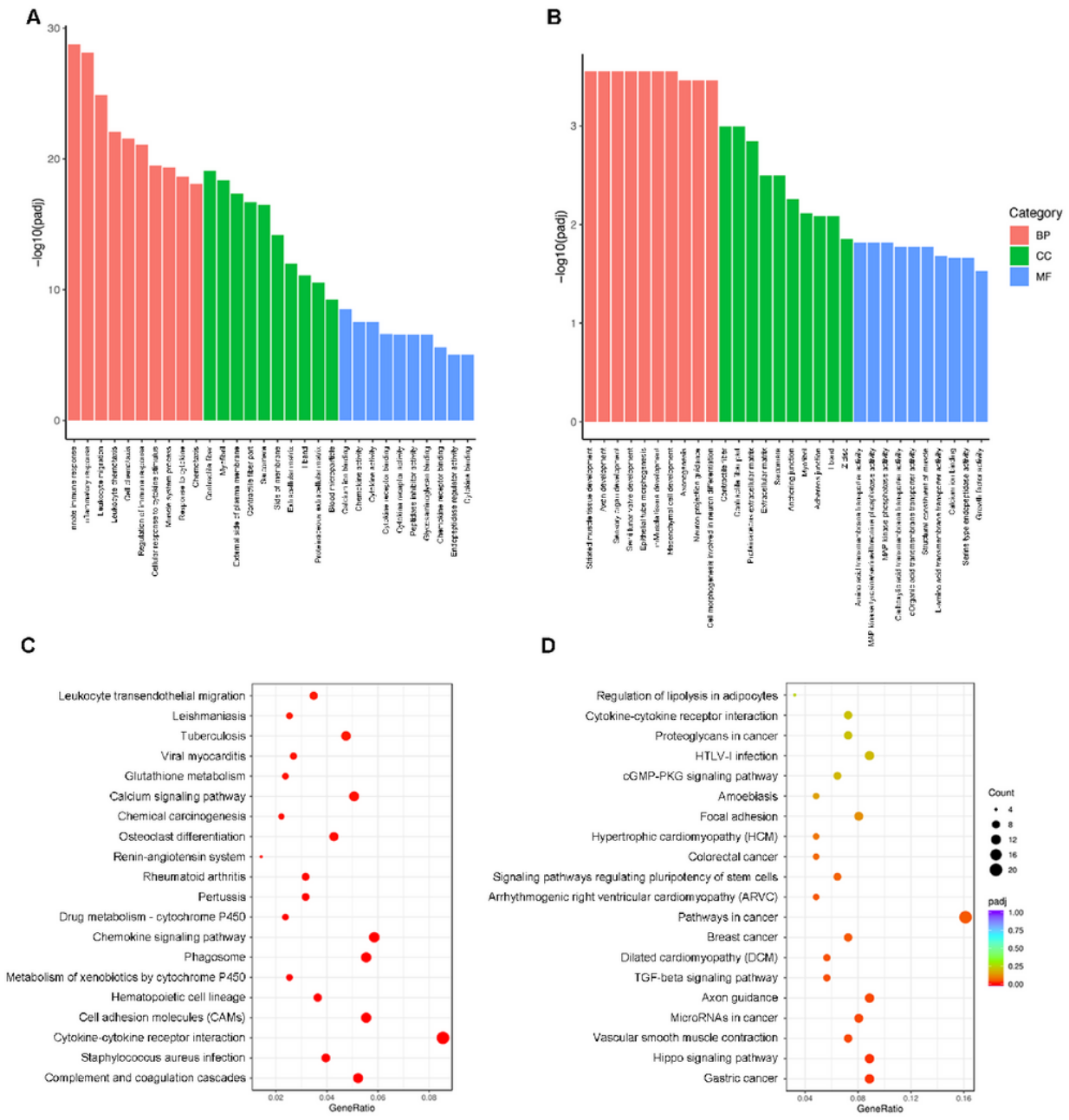

Figure 4

Enrichment results of up-regulated and down-regulated DEGs A, B GO enrichment of age-related DEGs. The top ten terms enriched for each category were listed. A Up-regulated genes enrichment; B Down-regulated genes enrichment. C, D KEGG pathway enrichment of age-related DEGs. The top twenty pathways enriched were listed. Count, differential gene count in indicated pathway; padj, adjusted P value of indicated pathway. C Up-regulated genes enrichment; D Down-regulated genes enrichment.

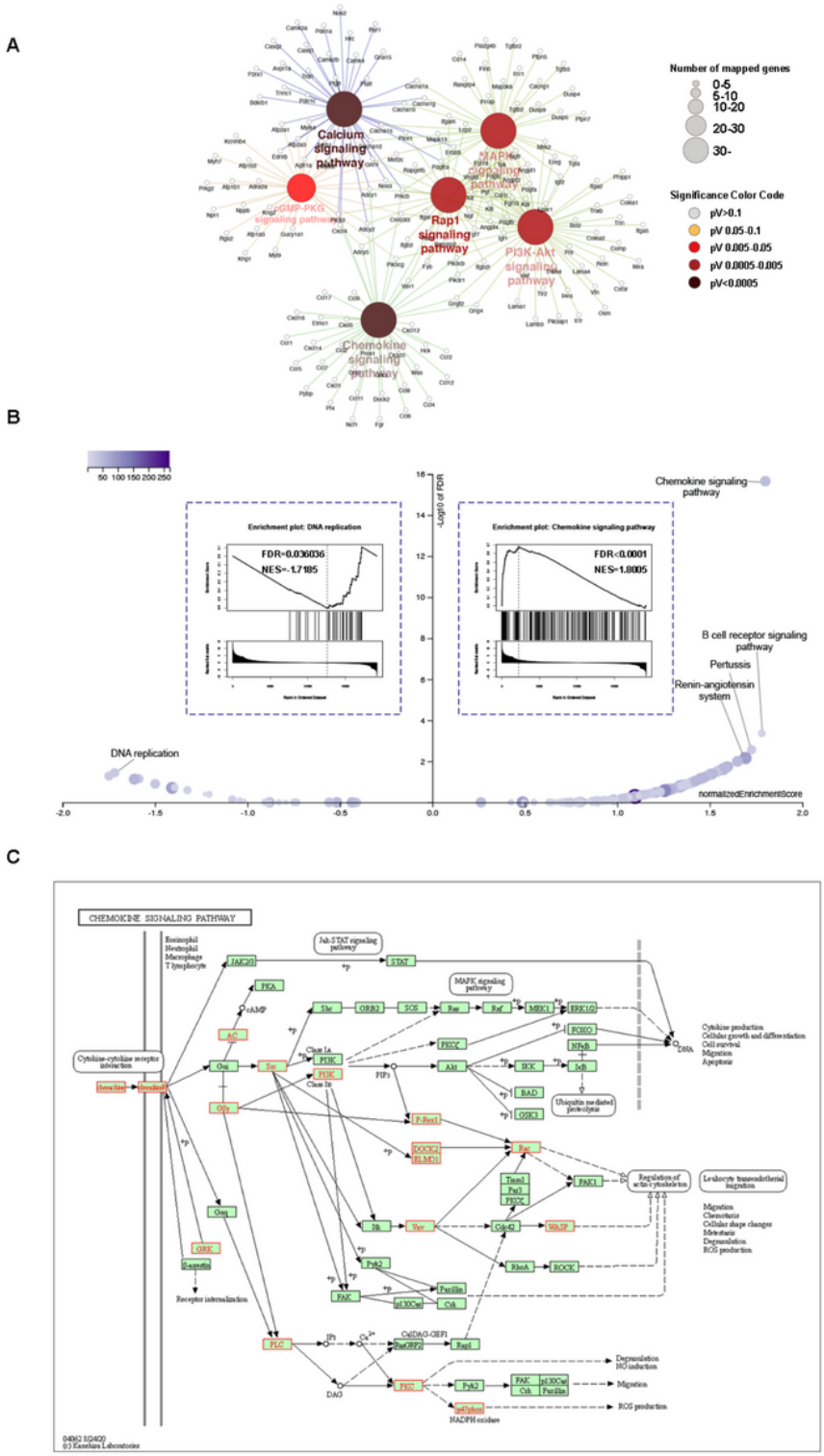

Figure 5

Enrichment results of overall DEGs A KEGG pathway enrichment of age-related DEGs. B Volcano and enrichment plot of GSEA in significance level at FDR < 0.05. NES, normalized enrichment score. FDR, false discovery rate. C Map of chemokine signaling pathway in KEGG database. Mapped DEGs were shown in red.

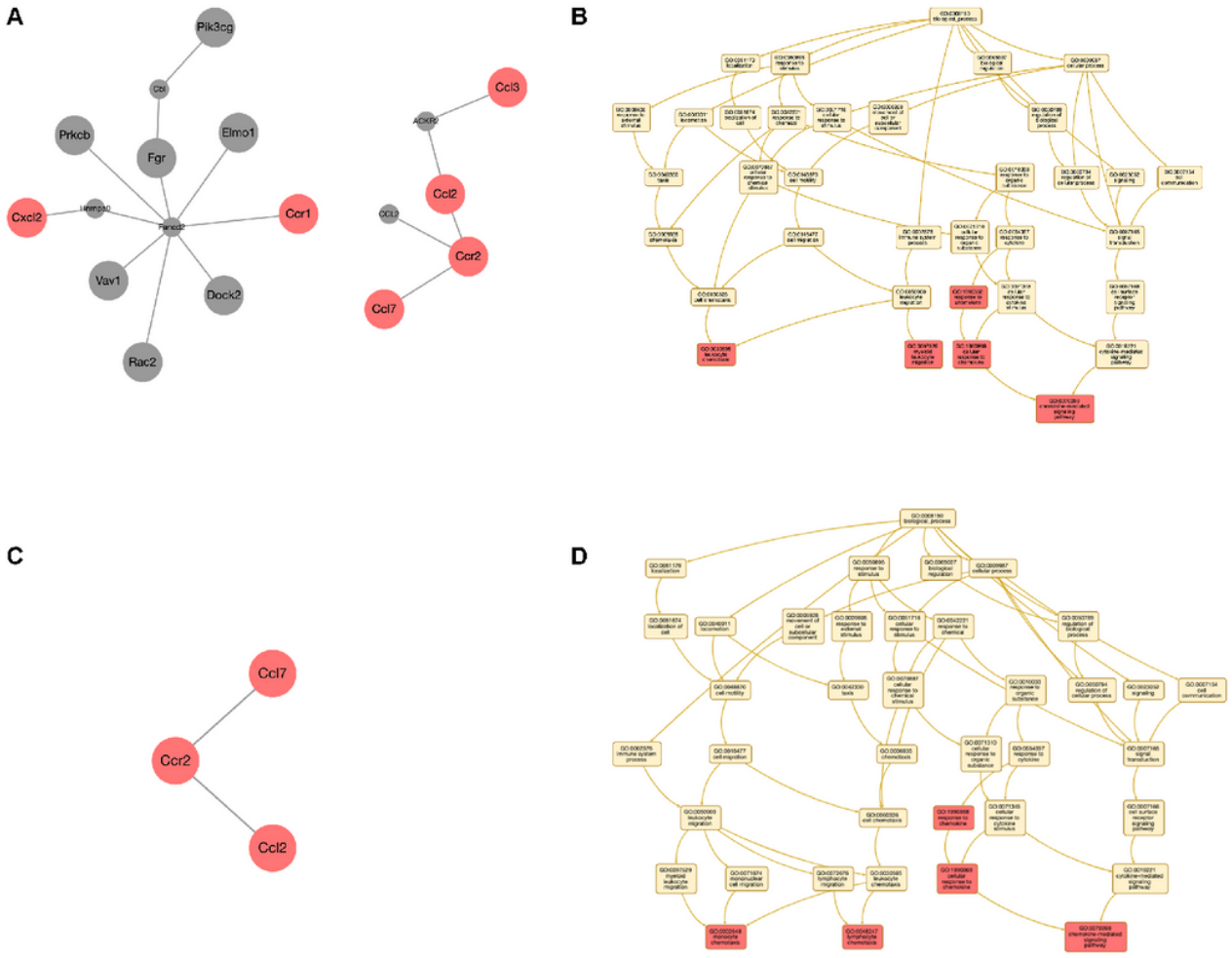

Figure 6

PPI network of DEGs mapped chemokine signaling pathway A Expanded PPI network of DEGs mapped chemokine signaling pathway. B Top 5 of GO BP categories that all seeds and top ranking neighbors in A could be enriched. C Retrieved PPI network of DEGs mapped chemokine signaling pathway. D Top 5 of GO BP categories that Ccl7, Ccl2, Ccr2 could be enriched.

Supplementary Files

This is a list of supplementary files associated with this preprint. Click to download.

- supplementalfiles.pdf